ELECTRIC AND MAGNETIC FIELDS FROM TWO-DIMENSIONAL ANISOTROPIC BISYNCYTIA

NESTOR G. SEPULVEDA AND JOHN P. WIKSWO, JR.
Department of Physics and Astronomy, Vanderbilt University, Nashville, Tennessee 37235

ABSTRACT Cardiac tissue can be considered macroscopically as a bidomain, anisotropic conductor in which simple depolarization wavefronts produce complex current distributions. Since such distributions may be difficult to measure using electrical techniques, we have developed a mathematical model to determine the feasibility of magnetic localization of these currents. By applying the finite element method to an idealized two-dimensional bisyncytium with anisotropic conductivities, we have calculated the intracellular and extracellular potentials, the current distributions, and the magnetic fields for a circular depolarization wavefront. The calculated magnetic field 1 mm from the tissue is well within the sensitivity of a SQUID magnetometer. Our results show that complex bisyncytial current patterns can be studied magnetically, and these studies should provide valuable insight regarding the electrical anisotropy of cardiac tissue.

INTRODUCTION

In the mid-1970's, a controversy arose in magnetocardiography research regarding the value of the magnetocardiogram (MCG). In a very simple model of cardiac activation, now termed the uniform double-layer model, the electrically active region can be approximated by a cup-shaped wavefront that propagates outward at up to 1m/s (1). It can be shown that both the electric and magnetic fields produced by such a source are determined by the rim of the cup, and thus one can argue that the two signals contain the same information but with differing spatial sensitivities. The uniform double-layer is an example of a source in which physiological constraints cause the electric and magnetic fields to be directly related and was used to explain why the MCG could contain no new information as compared with the electrocardiogram (ECG) (2). Moreover, it has been suggested that both the electric and magnetic field produced by active tissue share a common source at the level of a single cell (3). Such a suggestion, which remains to be proven, means that measurements of the external electric field completely determine the external magnetic field. However, by the late 1970's, it was becoming apparent that the uniform double-layer model was inadequate to explain the complexities in the cardiac depolarization wavefront that were revealed by careful measurements within millimeters of the wavefront (4–7). Therefore, in 1982, Wikswo and Barach devised a hypothetical wavefront that would be electrically indistinguishable from the conventional model but would have a differing magnetic field (8). By relaxing the assumption that the source currents are perpendicular to the cardiac activation wavefront, more interesting tangential current sources can be considered, such as might result from the spiral geometry of cardiac muscle fibers within the heart (9, 10). Since both of these sources have the same divergence, they will produce identical electric fields. The second source differs from the first only by a tangential, divergence-free current source component parallel to the wavefront surface. This component will cause the two sources to have differing curls and thus differing magnetic fields. Therefore only magnetic measurements could distinguish between such sources, if they indeed exist (8, 11). The existence of such sources in the heart has yet to be demonstrated with MCG measurements, although recent studies present quantitative evidence for new independent information in the MCG (12). Furthermore, a recent theoretical analysis (13) indicates that electrically silent magnetic fields may arise in some tissues, including cardiac tissue, implying that the magnetic fields may contain information that is absent in the electric potential. In this paper, we extend the scope of the information content discussion to include a two-dimensional bidomain model of cardiac tissue that accounts for different intracellular and extracellular anisotropies.

Address correspondence and offprint requests to Dr. John P. Wikswo, Jr., Department of Physics and Astronomy, Vanderbilt University, Box 1807 Station B, Nashville, TN 37235.

THEORY

Cardiac tissue is functionally a syncytium, and the analogy to a "three-dimensional cable" has been used by Jack et al. (14) to describe such a system in which current in an infinitesimal region of myocardium might be flowing in the interstitial space, the intracellular space, through the

membrane that connects them, or in any combination of the three. From a macroscopic perspective cardiac tissue can be viewed as a bidomain, or bisyncytium, where the intracellular and the extracellular media are treated as separate continuous conducting domains superimposed in space, yet separated by cell membrane everywhere (15, 16). Because of the cell geometry and the interconnections at the ends of cardiac cells, the intracellular space exhibits an anisotropic resistivity, with the low-resistance axis being parallel to the cell axis. However the geometry of the extracellular space differs from that of the intracellular space, so that the extracellular space generally exhibits an anisotropy different from that of the intracellular space. Thus, the electrical conductivities of the two domains have differing directional dependence (17, 18). Because of the differing anisotropy in the two spaces, depolarization currents flowing in the intracellular space will follow a path different from the extracellular return currents associated with the depolarization wavefront (19, 20). Since the bidomain model of cardiac tissue is continuous, rather than discrete or cellular, the potentials as well as the conductivities are average values over a volume containing many cardiac cells. In this approximation the equation of continuity of current for the bidomain model is written as

$$\nabla \cdot (\mathbf{J}_i + \mathbf{J}_e) = 0, \tag{1}$$

where $\mathbf{J}_i$ and $\mathbf{J}_e$ are the intracellular and the extracellular current densities, respectively. The transmembrane potential V_m is the difference between the intracellular (ϕ_i) and extracellular (ϕ_e) potentials

$$V_m = \phi_i - \phi_e. \tag{2}$$

It has been shown (16, 19) that the intracellular and the extracellular potentials are given by

$$\nabla \cdot \{(\tilde{\tilde{\sigma}}_i + \tilde{\tilde{\sigma}}_e)\nabla\phi_i\} = \nabla \cdot (\tilde{\tilde{\sigma}}_e \nabla V_m) \tag{3}$$

$$\nabla \cdot \{(\tilde{\tilde{\sigma}}_i + \tilde{\tilde{\sigma}}_e)\nabla\phi_e\} = -\nabla \cdot (\tilde{\tilde{\sigma}}_i \nabla V_m), \tag{4}$$

where $\tilde{\tilde{\sigma}}_e$ and $\tilde{\tilde{\sigma}}_i$ are the conductivity tensors describing the anisotropic extracellular and intracellular conductive media. From Eqs. 3 and 4 it is apparent that the origin of the extracellular and intracellular potentials is a volumetric distribution of current proportional to the gradient of the transmembrane potential. The use of the conductivity tensors $\tilde{\tilde{\sigma}}_i$ and $\tilde{\tilde{\sigma}}_e$ in Eqs. 3 and 4 is required because of the electrical anisotropy of cardiac tissue. If the conductivity tensors are referred to the axes of a right-hand rectangular coordinate system (x, y, z), then the conductivity tensors are diagonal and contain the components σ_x, σ_y, and σ_z, (we do not consider off-diagonal terms in the conductivity tensor, which may be associated with the spiral structure of certain regions of myocardium [13]). If the current densities $\mathbf{J}_i$ and $\mathbf{J}_e$, the extracellular potential ϕ_e, the intracellular potential ϕ_i, as well as the transmembrane potential V_m, are also referred to the same axes, then Eqs. 3 and 4 can be written for a two-dimensional bidomain as

$$(\sigma_{ix} + \sigma_{ex})\partial^2\phi_i/\partial x^2 + (\sigma_{iy} + \sigma_{ey})\partial^2\phi_i/\partial y^2 = \sigma_{ex}\partial^2 V_m/\partial x^2 + \sigma_{ey}\partial^2 V_m/\partial y^2 \tag{5}$$

$$(\sigma_{ix} + \sigma_{ex})\partial^2\phi_e/\partial x^2 + (\sigma_{iy} + \sigma_{ey})\partial^2\phi_e/\partial y^2 = -\sigma_{ix}\partial^2 V_m/\partial x^2 - \sigma_{iy}\partial^2 V_m/\partial y^2. \tag{6}$$

If the spatial variation of the transmembrane potential is known, and if appropriate boundary conditions are specified, the forward problem is the determination of the potential distributions, using Eqs. 5 and 6, given the cardiac conductivity values. The forward problem, which should give a unique solution, may be solved using numerical techniques. By assuming the existence of a circularly shaped isochrone action potential of radius R_u = 2.0 mm, given by

$$V_m(x, y) = 52.0 \tanh [5.4 (R_u - R)] - 38.0 \text{ mV}, \tag{7}$$

where $R = (x^2 + y^2)^{1/2}$, Plonsey and Barr (19) examined the resulting potential and current distributions in a two-dimensional anisotropic tissue and found that a circular depolarization wavefront will produce a current distribution resembling a clover-leaf, with intracellular currents flowing primarily in one direction, and the extracellular return currents that close the clover leaf flowing orthogonally. Recognizing that these currents could be detected directly, without penetrating the cardiac tissue, by a magnetometer pick-up coil configured as a clover-leaf, we have made finite element calculations of the current distributions due to a circular wavefront in a two-dimensional cardiac bidomain, and used these currents to calculate the magnetic field.

METHODS

The calculation by Plonsey and Barr (19) used a complicated integral approach that required various spatial transformations of the potentials and the evaluation of integrals that are singular at the selected field points. The use of the finite element method to solve Eqs. 5 and 6 does not require such transformations and does not involve (at least in this model) the evaluation of integrals that may be singular. The finite element method was originated for the analysis of the stress in complex structures and has been extended to many areas of mathematical physics and recently to biophysics (21–24). Its major advantage over other numerical techniques is its flexibility to deal with curved boundaries, as well as complicated source terms and boundary conditions. The essence of the finite element solution of Eq. 5 or Eq. 6 in the bidomain model of cardiac tissue is the subdivision of the field region into an assemblage of discrete "finite elements" and the approximation of the scalar potentials ϕ_i or ϕ_e in each element in terms of a limited number of parameters. The division procedure and approximation of the field variable, which is carried out locally over each finite element, results in matrix equations that relate the input variable at specified points, called the nodes, in the element to the output variable at the same points. The important feature of the finite element method is the ability to formulate solutions for individual elements before putting them together to represent the entire problem. The resulting elemental matrices are summed node by node, resulting in global matrix equations having the same form as the equations for an individual element. The resulting system of equations can be solved by an

appropriate procedure to obtain the values of the potentials. After the unknown nodal values of the potentials are found, it is possible to make additional calculations to obtain other important parameters such as isopotential contours, current densities, and lines of current flux.

We have solved Eqs. 5 and 6 separately with a finite element calculation for a two-dimensional anisotropic bidomain model of cardiac tissue of infinite extent, obtaining extracellular and intracellular potentials. Boundary conditions were chosen such that $\phi_e = 0.0$ and $\phi_i = -90$ mV at infinity. Even though Plonsey and Barr used a square block of tissue for their calculations, the circularly centered source term suggests the use of a piece of tissue with a similar geometrical shape for a finite element calculation (although it is not necessary). For our calculations we have used a circular block of cardiac tissue. By reasons of symmetry it is necessary to analyze only one quadrant of the space. Standard eight-node quadrilateral and six-node triangular isoparametric finite elements (25, 26) were automatically generated in a circular region of radius 4 mm, using a special grid generation subroutine. To account for the specified boundary conditions at infinity, special "infinity" elements (27, 28) were also automatically generated at the outer border of the circular region. The model, shown in Fig. 1, has a total of 670 elements (40 being six-node triangles, 590 eight-node quadrilaterals, and 40 infinity elements) and a total of 2,073 nodal points. The conductivities, shown in Table I, were the same as used by Plonsey and Barr (19). The "nominal" case corresponds to typical values of myocardial conductivities. In the "reciprocal" case the extracellular conductivity in the x and y directions equals the intracellular conductivity in the y and x directions, respectively. We use Plonsey and Barr's activation wavefront, given by Eq. 7, which extends approximately from a radius of 1.5 to 2.5 mm.

TABLE I
CONDUCTIVITY VALUES*

Conductivity	Isotropic	Nominal	Reciprocal
	S/mm	*S/mm*	*S/mm*
σ_{ix}	1×10^{-4}	2×10^{-4}	2×10^{-4}
σ_{iy}	1×10^{-4}	2×10^{-5}	2×10^{-5}
σ_{ex}	1×10^{-4}	8×10^{-4}	2×10^{-5}
σ_{ey}	1×10^{-4}	2×10^{-4}	2×10^{-4}

*Data from Plonsey and Barr (19).

ELECTRICAL POTENTIALS AND CURRENTS

Fig. 2 is a plot of the radial dependence along the x and y axes of the calculated intracellular and extracellular potentials and the calculated transmembrane potential given by Eq. 2. Superimposed on the calculated transmembrane potential is the theoretical value given by Eq. 7. A comparison of the theoretical and calculated values for a few points along the y-axis for reciprocal anisotropy is shown in Table II. Errors were, in general, <0.3% at any point.

Fig. 3 shows the calculated intracellular and extracellular isopotential contours (Sepulveda, N. G., and C. F. Walker, manuscript submitted for publication) for isotropic, nominal, and reciprocal resistivities. In the isotropic case, shown in Fig. 3, *a* and *b*, the isopotentials are aligned with the wavefront, consistent with the uniform double-layer model. The extracellular potentials in the nominal case (Fig. 3 *d*) are small, covering a range of only few millivolts in the outer region starting at the center of the wavefront. The intracellular potentials (Fig. 3 *c*), which would be much harder to measure, are larger. The pattern

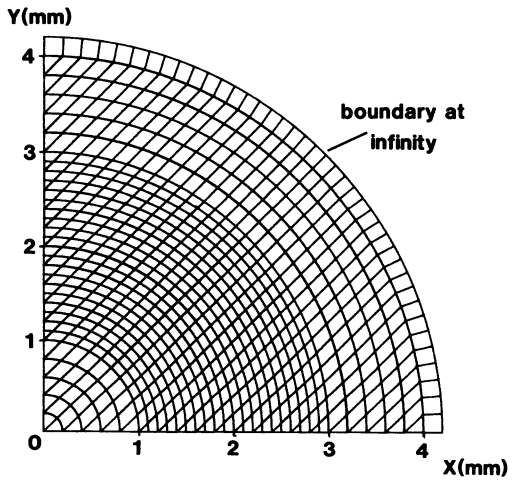

FIGURE 1 Finite element grid for a quadrant of a bidomain model of cardiac tissue. Note the "infinity elements" along the circumference of the grid.

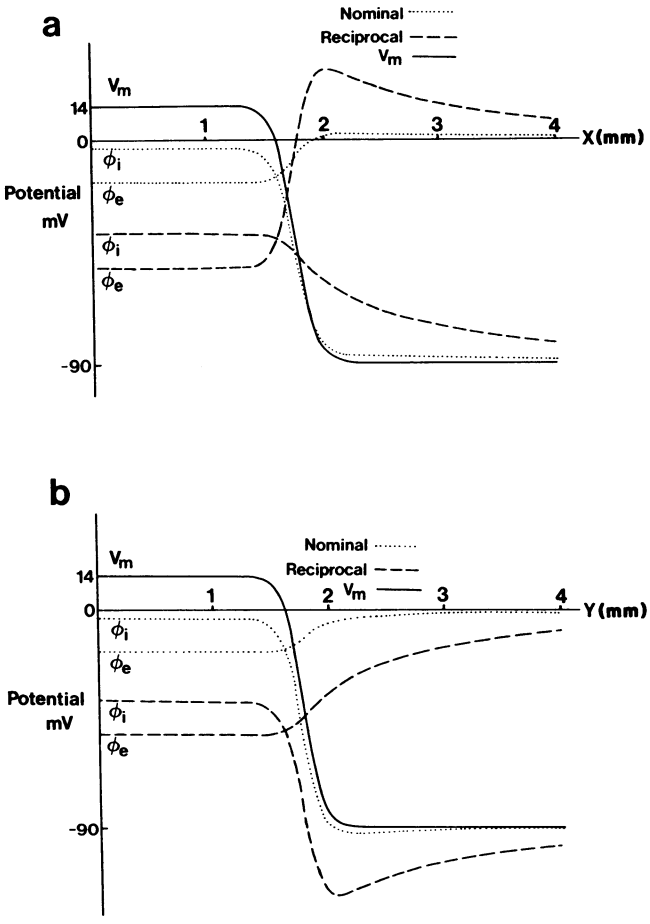

FIGURE 2 Calculated intracellular, extracellular, and transmembrane potentials (*a*) along the x axis and (*b*) along the y axis. V_m is given by Eq. 7 and describes a 1-mm thick activation wavefront with a 2-mm radius.

TABLE II
CALCULATED AND THEORETICAL POTENTIALS: RECIPROCAL CONDUCTIVITY CASE

Distance ($y = 0.0$)	Calculated values			Theoretical value	Difference
r	ϕ_i	ϕ_e	V_m	V_m	
mm	*mV*			*mV*	%
0.20	−37.98810	−51.98770	13.99960	14.00000	0.0028
1.00	−37.69280	−51.69010	13.99730	13.99788	0.0041
1.60	−38.40240	−51.01940	12.61700	12.63497	0.1422
1.90	−59.67580	−47.34330	−12.33200	−12.36463	0.2592
1.95	−69.91620	−45.57390	−24.34230	−24.29151	−0.2090
2.00	−81.37960	−43.46810	−37.91150	−38.00000	0.2328
2.05	−92.89110	−41.10150	−51.78960	−51.70849	−0.1568
2.40	−116.69300	−28.05190	−88.64110	−88.63497	−0.0069

of the extracellular and intracellular isopotential contours noticeably depart from the uniform double-layer in the outer region. In the reciprocal case the isopotential contours for both the intracellular (Fig. 3 *e*) and extracellular (Fig. 3 *f*) domains are larger in value than in the nominal case and they also differ markedly from those of the uniform double layer. The pattern of the isopotentials for nominal and reciprocal anisotropies suggests a complicated path for the flow of current, which cannot be determined from the isopotential contours alone since in the anisotropic case the direction of the flow of current at a point does not lie along the normal to the isopotential through the point.

Fig. 4 is a plot of the calculated intracellular and extracellular current vectors for isotropic, nominal, and reciprocal anisotropy. Each vector shows the relative magnitude and direction of the depolarizing current at the centroid of each element of the mesh. In a conventional uniform double-layer model with isotropic conductivities, the vectors are radial (Fig. 4, *a* and *b*), showing that the intracellular current moves toward the outside of the depolarizing wavefront. However, in the anisotropic bidomain model the current has a component tangential to the wavefront along the entire front. In the nominal case, the flow of current has a preferential path in the x-direction, for both the intracellular and the extracellular spaces as shown in Fig. 4, *c* and *d*. For the reciprocal case the flow of current takes a preferential y-direction in the extracellular space, whereas it takes a preferential x-direction in the intracellular space, as can be seen in Fig. 4, *e* and *f*. The current distributions in Fig. 4, *c–f* are noticeably different from the more commonly seen current distributions described by Laplacian potentials in isotropic, monodomain conductors. This difference is the result of the ability of current to vanish locally from one domain and reappear at the same location of the other domain.

The solenoidal nature of the total current is required by the statement of current continuity in Eq. 1 and can be demonstrated, for the nominal and reciprocal cases, by drawing the current lines of the total current density vector. It is known that the current lines of a current density vector $\mathbf{J}(x, y)$ are the solution of the differential equation

$$\partial y/\partial x = J_y/J_x, \tag{8}$$

where J_x and J_y are the components of the current density vector in the x and y directions, respectively. Eq. 8 was solved numerically for the nominal and reciprocal cases using a recently developed technique (Sepulveda, N. G., and J. P. Wikswo, Jr., manuscript submitted for publication). It can be seen from Fig. 5 that closed loops of current exist, which confirms the solenoidal property of the total current. As expected, the current loops for reciprocal anisotropy, in Fig. 5 *b*, have reflection symmetry about a line at an angle of 45° from the x and y axes. This figure also demonstrates the extent of current spread outside of the wavefront. It should be noted that the current lines within the wavefront are aligned with it, and they do not have the "staircase" configuration in the vicinity of the source region that resulted from the calculation technique of Plonsey and Barr (19). Otherwise, our calculation confirms the Plonsey–Barr results.

MAGNETIC FIELDS

The closed-loop current pattern shown in Fig. 5 suggests that one of the best methods to detect this type of electrical behavior may be to measure the magnetic field produced by the currents. The intracellular and extracellular currents were determined from the gradients of the potentials, and the net current $\mathbf{J}$ was calculated as

$$\mathbf{J} = \mathbf{J}_e + \mathbf{J}_i. \tag{9}$$

The law of Biot and Savart,

$$\mathbf{B}(\mathbf{r}) = \mu_0/4\pi \int_v \mathbf{J}(\mathbf{r}') \times (\mathbf{r} - \mathbf{r}')/|\mathbf{r} - \mathbf{r}'|^3 \, d^3\mathbf{r}', \tag{10}$$

was used to calculate the magnetic field component normal to the plane at distances of 1, 2, 4, 8, and 16 mm from the bisyncytial tissue. The calculation of the normal component is based upon the fact that SQUID magnetometers that measure the normal component of the magnetic field are easier to build than are ones that measure the tangential component. It should be pointed out that in the evaluation of the magnetic field it is necessary to consider the currents flowing in all the four quadrants. The magnetic field has a direction so that it points out of the page in quadrants I and III, with an opposite direction in quadrants II and IV. Due to the symmetry reasons the normal component of the magnetic field was calculated only for quadrant I. There is no magnetic field in the isotropic case, since the intracellular and extracellular currents are everywhere equal in strength and opposite in direction. The calculated iso-field contours for the magnetic fields produced by tissue with nominal and reciprocal anisotropies are similar in shape, but differ in magnitude. Fig. 6 shows the isocontours 1 mm above the tissue for nominal and reciprocal anisotropy; the peak field is 0. 28 nT for nominal

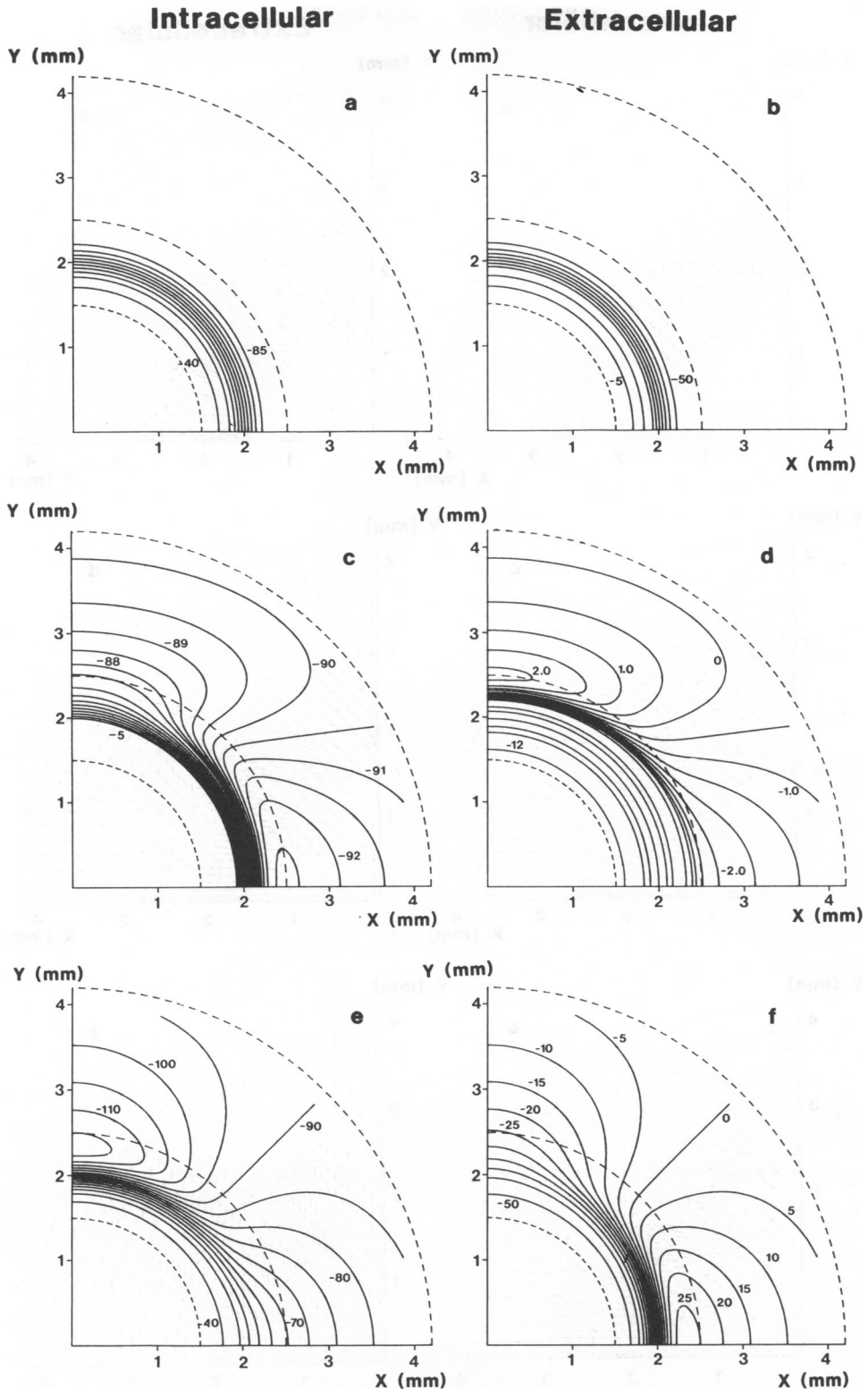

FIGURE 3 Intracellular and extracellular isopotential contours in millivolts for a 4-mm diam, 1-mm wide cardiac activation wavefront (shown by the dotted circles) in bisyncytial tissue with isotropic conductivities (*a* and *b*), nominal anisotropy (*c* and *d*), and reciprocal anisotropy (*e* and *f*).

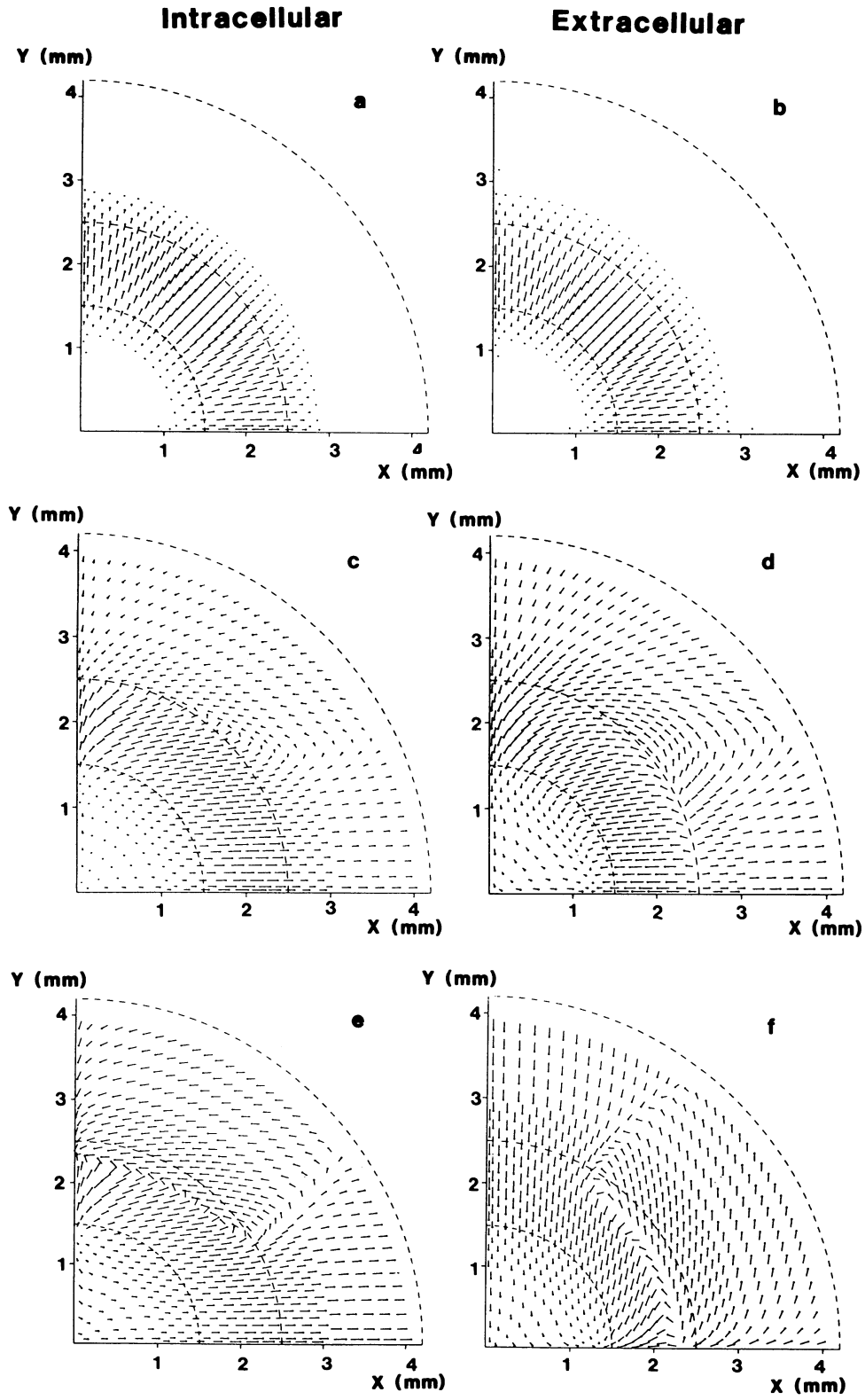

FIGURE 4 The calculated (*a*) intracellular and (*b*) extracellular current distributions for isotropic conductivities, (*c* and *d*) for nominal anisotropy, and (*e* and *f*) for reciprocal anisotropy. Current density vector magnitudes are represented by arrows whose lengths have been scaled logarithmically.

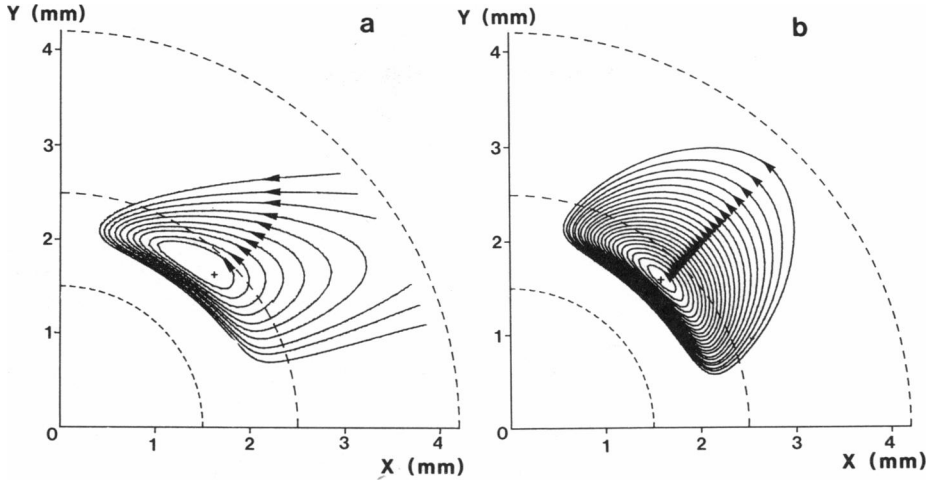

FIGURE 5 Current lines for the total (or net) current with (*a*) nominal anisotropy and (*b*) reciprocal anisotropy. The starting points of the current lines were calculated by assigning 10 μA/line. The cross mark is the reference point for calculation of the starting points for each line.

anisotropy and 1.07 nT for reciprocal. In both cases the peak is located at the leading edge of the wavefront, shown by the inner cross mark, and we see that the clover-leaf current pattern predicted by Plonsey and Barr is manifested as a distinctive magnetic field pattern consistent with a planar magnetic octapole. The strength of the octapole is determined by the anisotropies of the intracellular and extracellular spaces, so that magnetic measurements may provide a unique way not only to detect the currents but also to determine quantitatively the cellular anisotropy.

Fig. 7 shows a logarithmic plot of the variation of the peak of the magnetic field as a function of the distance from the center of the bidomain for nominal and reciprocal anisotropies. It can be seen that in both cases the magnitude of the magnetic field varies inversely with approximately the fourth power of the distance as expected for an octapole distribution and that the absolute magnitude of the field is determined by the relative anisotropies of the intracellular and extracellular spaces.

DETERMINATION OF CONDUCTIVITIES FROM ELECTRIC AND MAGNETIC MEASUREMENTS

The results obtained for nominal and reciprocal anisotropies have shown that in the two-dimensional bidomain model of cardiac tissue a simple depolarization wavefront produces potential and current distributions that depart markedly from those of the uniform double-layer model of cardiac activation. We also calculated the intracellular and extracellular potentials using the equal anisotropy ratio conductivities: $\sigma_{ix} = 3.43 \times 10^{-4}$, $\sigma_{iy} = 5.96 \times 10^{-5}$, $\sigma_{ex} = 6.25 \times 10^{-4}$, and $\sigma_{ey} = 1.09 \times 10^{-4}$ (S/mm) (29). The

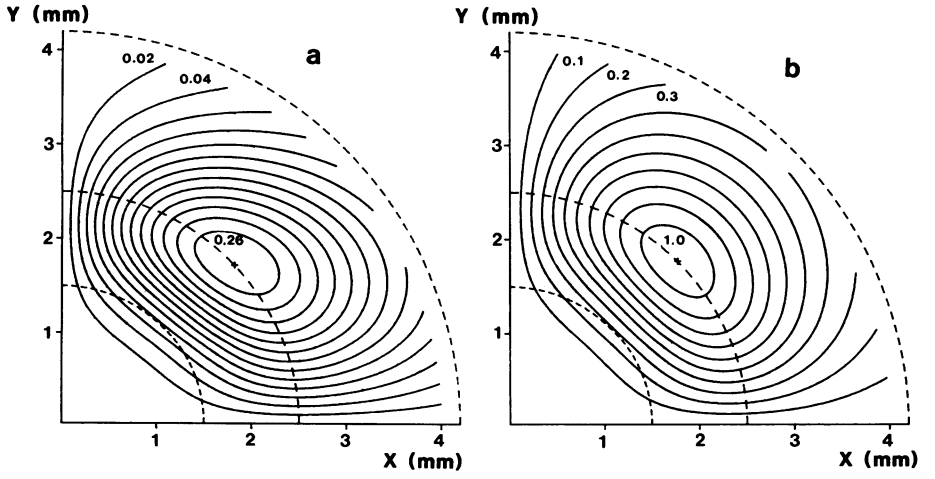

FIGURE 6 The isofield contours in nT for the normal component of the magnetic field 1 mm above a circular depolarization wavefront in a cardiac bisyncytium (*a*) nominal anisotropy, (*b*) reciprocal anisotropy.

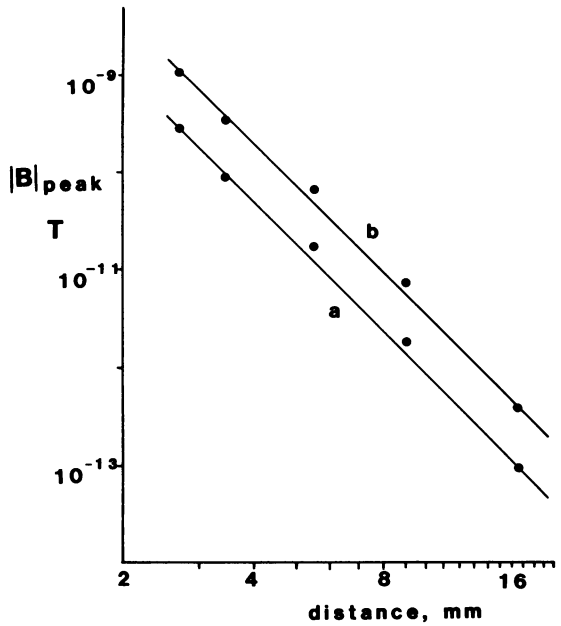

FIGURE 7 Variation of the peak magnitude of the magnetic field as a function of the distance from the center of the bidomain: (*a*) nominal anisotropy, (*b*) reciprocal anisotropy.

resulting patterns of the intracellular and extracellular isopotential contours (not shown) also depart markedly from those of the uniform double-layer model. As expected no closed-current loops were detected for this particular situation and the resulting magnetic field was zero. Thus, regardless of the anisotropy ratios, we found patterns of complex potential distribution and in certain cases strong magnetic fields. Since both the transmembrane potential V_m and the boundary conditions are the same in the isotropic, nominal, reciprocal, and equal anisotropy ratio cases, it is evident that the potential and current distributions are strongly dependent on the conductivity values chosen in the solution of Eqs. 5 and 6. One of the most important aspects of our bidomain model is that under a given set of conditions, those potential and current distributions can be predicted with ease. This suggests that a complete characterization of potentials and magnetic fields over a range of normal conductivities will allow the bidomain model to be useful in interpreting and explaining some features of normal and abnormal cardiac conduction.

The determination of cardiac conductivities from a knowledge of measured potentials and currents and the adoption of a model to describe cardiac tissue can be considered as an inverse problem. Recently, Plonsey and Barr (29) provided a review of the models that have been used in the determination of cardiac conductivities from measured potentials and injected currents. They have shown that the same measurements can lead to different calculated results depending upon the model used to describe cardiac tissue. On the basis of such analysis and comparisons, the conductivity values obtained using monodomain models can be rejected since they do not describe correctly cardiac tissue behavior. Cardiac conductivity values obtained using an isotropic bidomain can also be discarded, since, as indicated before, this model fails to predict correctly the potential fields generated by a wavefront spreading in cardiac tissue. On the other hand, the use of a bidomain model with equal anisotropy ratios ($\sigma_{ex}/\sigma_{ix} = \sigma_{ey}/\sigma_{iy}$) allows the determination of analytical relationships between the measurements (using the four-electrode technique) and the cardiac conductivities (29). However, the assumption of equal anisotropy ratios may not be valid and the results obtained, even though better estimates of the macroscopic conductivities of the actual structure, are still in doubt. We will now show how our model might be coupled with extracellular electric and magnetic measurements of propagating activation wavefronts to provide a more accurate determination of the intracellular and extracellular anisotropic conductivities.

From the perspective of the inverse problem, it is important to note that the same potential distribution can be obtained by adjusting the cardiac conductivities such that both sides of Eqs. 5 and 6 are multiplied by the same constant C. In these cases the magnetic field, if different from zero (i.e., unequal anisotopy ratios) changes by the constant C. On the other hand, it is possible to obtain the same current distribution by adjusting conductivities such that the magnetic field remains the same ($\sigma_{ex} = \sigma_{ey} - 1.0$ S/mm and $\sigma_{iy} = \sigma_{ix} - 1.0$ S/mm are expressions that can be used to determine values of conductivities that give the same magnetic field). In these cases the potential distribution changes. Thus, an inverse calculation of conductivities using electric potentials alone would be indeterminant to within the constant C multiplying all conductivities, while an inverse calculation using magnetic fields alone would be indeterminant with regard to certain combinations of the conductivities. For this reason, it appears that it would be difficult to infer the true anisotropy of cardiac tissue at the activation wavefront by using either electric or magnetic measurements alone. However, a combined electric and magnetic analysis should allow unique determination of all four conductivities. This determination would not require injection of current into the tissue, but would measure the impedances seen by the actual cardiac activation wavefront.

The magnetic field may prove useful in assessing the validity of the equal anisotropy models. Closed-loop current patterns arise in a bidomain model only when the anisotropy ratios are different. These closed-loop currents manifest themselves by their magnetic field. Thus, it should be possible to design experiments to look for those currents using a magnetometer. If magnetic fields associated with those currents are detected one can conclude that the tissue has unequal anisotropies, and models with equal anisotropy ratios will produce erroneous results. If no magnetic fields are found to be associated with the currents, the assumption of equal anisotropy ratios will be

confirmed and experimental determination of conductivity would be vastly simplified. Until a characterization of the true macroscopic anisotropy of cardiac tissue can be made, any conclusions about average cardiac conductivities should be viewed with caution.

As a first step toward the goal of combined electrical and magnetic characterization of cardiac tissue, we consider the way in which the potential distribution and the magnetic field vary as a function of cardiac conductivity values. We consider, for the remainder of our discussion, that cardiac tissue is described by a totally anisotropic bidomain model and we assume that the nominal conductivity values represent "normal" cardiac tissue. We performed calculations in which three conductivity values were maintained at the nominal value, whereas the fourth value was varied to half and twice the nominal value. Table III shows the calculated upper and lower limits for the extracellular and intracellular potential distributions. Even though quantitatively there were differences in the potential distributions, the patterns of those distributions, as determined from the isopotential contours (not shown), remain similar to those of the nominal case. A twofold increase in σ_{ix} produces a marked increase in the range of extracellular potentials, in which the intracellular medium becomes much more negative. Very similar results are obtained by decreasing σ_{ex} by half the nominal value. Reduction in σ_{ix} by half is manifested by a decrease in the range of the extracellular potentials. Furthermore, the intracellular medium becomes slighly less negative. A twofold increase in σ_{ex} produces changes in the extracellular potentials similar to those obtained by halving σ_{ix}. However, the variation in the intracellular potentials toward less negative values is more pronounced than that obtained at half σ_{ix}. A twofold increase in σ_{iy} is manifested by a decrease in the range of the intracellular potentials and the extracellular potentials become more negative. Very similar results are obtained by decreasing σ_{ey} by half. Reduction in σ_{iy} by half is accompanied by an increase in the range of intracellular potentials, while the extracellular medium becomes less negative. Similar results are obtained by a twofold increase in σ_{ey}. Thus, we conclude that changes in the cardiac conductivity values will have marked effects in the intracellular and extracellular potential distributions. Abnormal extracellular potentials that have been observed during certain pathological states (30) can be explained, in principle, by changes in cardiac conductivity values, and our numerical results may help in the understanding and interpretation of such observations. However a correlation between those pathological cardiac conditions and the corresponding changes in intracellular and extracellular cardiac conductivities remains to be determined and deserves further study.

TABLE III
EXTREME POTENTIAL VALUES AND PEAK MAGNETIC FIELD

Conductivity (N‡)	Extreme potential values				Peak magnetic field
	Extracellular		Intracellular		
	mV				nT
σ_{ix}					
2 × N	−28.81	4.29	−96.34	−14.28	0.6655
1 × N	−17.88	2.10	−92.60	−3.69	0.2793
0.5 × N	−10.98	0.38	−90.38	−3.04	0.0496
σ_{iy}					
2 × N	−19.86	0.62	−90.68	−5.81	0.0900
1 × N	−17.88	2.10	−92.60	−3.69	0.2793
0.5 × N	−16.83	2.91	−93.76	−2.54	0.3791
σ_{ex}					
2 × N	−11.17	0.26	−90.29	2.86	0.5053
1 × N	−17.88	2.10	−92.60	−3.69	0.2793
0.5 × N	−26.28	5.94	−97.27	−11.94	0.0638
σ_{ey}					
2 × N	−15.19	3.94	−94.31	−1.01	0.0578
1 × N	−17.88	2.10	−92.60	−3.69	0.2793
0.5 × N	−20.18	0.42	−90.52	−6.10	0.5721

*The spatial position of the extreme potential values and the peak magnetic field do not necessarily coincide with the spatial position for the nominal case.
‡N, nominal value (see Table I).

As evidence of the sensitivity of the magnetic fields to the conductivities, Fig. 8 shows the strength of the normal component of the magnetic field as a function of conductivities. These curves have been obtained by calculating the magnetic field at the same spatial location (which corresponds to the location 1 mm above the bidomain at which the peak value for the nominal case was calculated). Very similar results were obtained at other locations. It should be noted that comparable changes in the magnetic field are produced by changes in σ_{ix} and σ_{ey}, as well as by σ_{iy} and σ_{ex}.

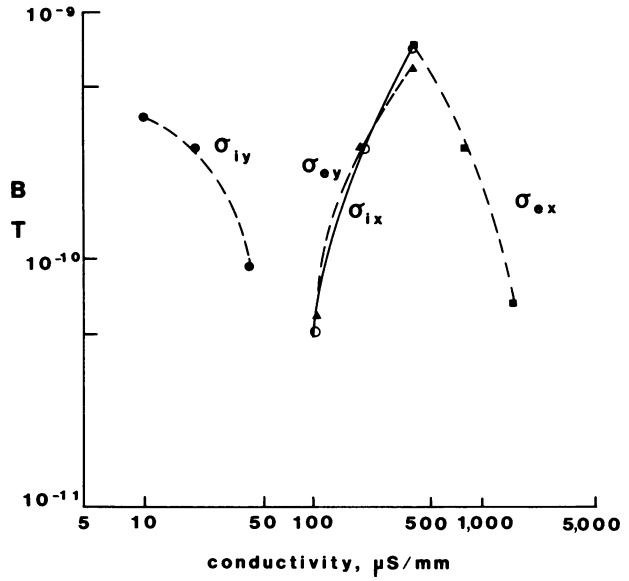

FIGURE 8 Variation of the magnetic field at a point as a function of conductivity values.

It should also be noted that as the anisotropy ratios tend toward being equal, the magnetic field approaches to zero.

In a real experiment the intracellular and extracellular potentials can be measured using an array of electrodes mounted in fixed positions, while the magnetic field can be measured with a SQUID magnetometer positioned directly above the tissue. These measurements are prone to many different errors or uncertainties. In a well controlled experiment many of the factors contributing to erroneous measurements, such as calibration errors, errors due to the presence and finite dimensions of the electrodes and coils, errors due to movement of the sensors from their fixed positions, etc., can be removed or at least accounted for. The remaining error present in the comparison of measurements with a model can be considered as random and must be ascribed to the uncertainty, or variation, of the variables being determined, in our case the four conductivities. It is well known that such errors can be described and analyzed by a proper application of statistical methods. To minimize the uncertainty in the calculated conductivity values, we must first ask what measurements present the greatest sensitivity to conductivity changes in the study of cardiac tissue and would thereby be best for determination of these conductivities. Although an exhaustive study has not been performed, Table IV provides some insights into this question by tabulating the coefficients of sensitivity for the intracellular and extracellular potentials and magnetic fields measurements. We assume that we would solve the inverse problem by performing a least-square-fit of the data calculated using our bidomain model to the measured data, with the model parameters adjusted to provide the best fit. We define the coefficient of sensitivity for such a fit as

$$C = \sum^{n} (X_{ei} - X_{mi})^2 \Big/ \sum^{n} (X_{ei})^2, \qquad (11)$$

TABLE IV
SENSITIVITY COEFFICIENTS FOR AN ARRAY OF NINE SENSORS

Conductivity change* %	Sensitivity coefficients		
	Intracellular	Extracellular	Magnetic
σ_{ix}			
−20	4.67×10^{-4}	2.20×10^{-2}	9.97×10^{-2}
+20	4.08×10^{-4}	1.93×10^{-2}	9.02×10^{-2}
σ_{iy}			
−20	2.00×10^{-5}	9.44×10^{-4}	1.98×10^{-2}
+20	1.91×10^{-5}	9.08×10^{-4}	1.93×10^{-2}
σ_{ex}			
−20	4.76×10^{-4}	2.25×10^{-2}	7.04×10^{-2}
+20	2.72×10^{-4}	1.28×10^{-2}	4.53×10^{-2}
σ_{ey}			
−20	5.96×10^{-5}	2.82×10^{-3}	8.12×10^{-2}
+20	4.05×10^{-5}	1.90×10^{-3}	6.45×10^{-2}

*From the nominal value.

where X_{ei} corresponds to an "exact" measurement at a point i that represents the data provided by the tissue under test, X_{mi} corresponds to model data with the uncertain values of the conductivities, and n is the number of sampled points. For the exact measurements we have used the potentials or magnetic field calculated using the nominal conductivity values. In a real experiment these data would be the actually measured potentials and fields produced by a system with unknown conductivities. Potential and magnetic field data with "uncertainties" were calculated by setting three conductivities equal to the nominal values and by varying the remaining one by ±20% about its nominal value. The sensitivity coefficients for the intracellular and extracellular potentials were calculated using the potential values at nine points that correspond to a hypothetical array of electrodes placed on the cardiac tissue as shown in Fig. 9. The magnetic sensitivity coefficient was obtained using the values of the normal component of the magnetic field calculated at the same (x, y) coordinates of the nine points but 1 mm above the bidomain. The results tabulated in Table IV show that in each case the magnetic sensitivity coefficient has the highest value and that the intracellular potential sensitivity coefficient has the lowest value. Similar results were obtained using more data points. These results indicate that the intracellular potentials are quite insensitive to conductivity changes. These results also agree with the emphasis given by Spach et al. (5) to extracellular measurements, rather than intracellular recording, for the purpose of studying propagation in anisotropic cardiac muscle. The results also demonstrate that magnetic measurements are much more sensitive to changes in conductivity values, and would thereby produce fits of model to experiment with the least uncertainty in conductivity. This in turn suggests that magnetic recording may provide a better technique for the study of anisotropy in cardiac muscle.

We also examined the fit of a combination of extracellular potentials and magnetic fields. While slight increases in

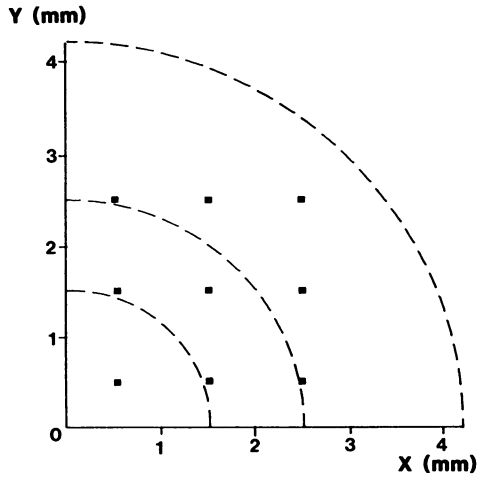

FIGURE 9 Sensor positions for determination of sensitivity coefficients.

sensitivity were seen for the combined data, the results were dominated by the magnetic measurements. This occurred because the magnetic analysis had a substantially higher sensitivity than the electrical analysis, and we weighted electric and magnetic data equally. In practice differences in signal-to-noise ratio would be taken into account and if electric data had a higher signal-to-noise ratio than the magnetic its contribution would be increased. Since our simulated search for the best fit involves the variation of only a single conductivity at the time, we did not observe the indeterminancy in the electric-alone or magnetic-alone inverse calculation, nor did we see the removal of the indeterminancy with the combined analysis. This effect would of course be significant in a minimization search that allowed all four conductivities to vary simultaneously.

SUMMARY

The results obtained using the finite element method confirm the prediction by Plonsey and Barr that in two-dimensional anisotropic tissue simple depolarization wavefronts produce complex current distributions. The ease, detail, and accuracy with which we can calculate the potentials, currents, and magnetic fields demonstrate the capabilities of the finite element technique for the calculation of bioelectric currents in two-dimensional bisyncytia. Even more complex distributions would be expected in three dimensions, and the finite element technique should be equally applicable.

These complex, closed-loop current distributions may be important for arrhythmia reentry and fibrillation, but it will be difficult to detect with electrical measurements because the insertion of electrodes will disrupt the tissue and the deviation in the external potentials are not large. Our calculation shows that the current distributions produce a characteristic magnetic field pattern whenever the two domains have differing anisotropy ratios, and that this field could be readily detected with a high resolution SQUID magnetometer. The unique magnetic signature of these closed-loop current patterns provide a potentially powerful tool for studying cardiac activation.

The bidomain model of cardiac tissue provides a tool that can be explored and used to study and explain features of cardiac conduction. However, it should be remembered that "a model is valid when it measures what it is intended to measure" (31). Thus, experimental data must be used to evaluate the validity of the bidomain model. This evaluation must involve comparison of the model's predictions not only with measured intracellular and extracellular potentials but also with the measured magnetic fields. When the applicability of the bidomain model to a particular cardiac preparation and the validity and reliability of our calculations have been determined experimentally, this mathematical approach should then provide a new technique for analyzing normal and pathological cardiac activation.

The comments of Leonora Wikswo and Brad Roth are gratefully acknowledged.

This research has been supported in part by Office of Naval Research Contract N00014-82-K-0107 and by a grant from Cardiac Pacemakers Inc. Computer time was provided by the College of Arts and Science, Vanderbilt University.

Received for publication 19 August 1986 and in final form 24 November 1986.

REFERENCES

1. Frank, E. 1953. A comparative analysis of the eccentric double-layer representation of the human heart. *Am. Heart J.* 46:364–378.
2. Rush, S. 1975. On the independence of magnetic and electric body surface recordings. *IEEE (Inst. Electr. Electron. Eng.) Trans. Biomed. Eng.* 22:157–167.
3. Plonsey, R. 1982. The nature of sources of bioelectric and biomagnetic fields. *Biophys. J.* 39:309–312.
4. Corbin, L. V., and A. M. Scher. 1977. The canine heart as an electrocardiographic generator: dependence on cardiac cell orientation. *Circ. Res.* 41:58–67.
5. Spach, M. S., W. T. Miller III, E. Miller-Jones, R. B. Warren, and R. C. Barr. 1979. Extracellular potentials related to intracellular action potentials during impulse conduction in anisotropic canine cardiac muscle. *Circ. Res.* 45:188–204.
6. Spach, M. S., W. T. Miller III, D. B. Geselowitz, R. C. Barr, J. M. Kootsey, and E. A. Johnson. 1981. The discontinuous nature of propagation in normal canine cardiac muscle. Evidence for recurrent discontinuities of intracellular resistance that affect the membrane currents. *Circ. Res.* 48:39–54.
7. Colli-Frazone, P., L. Guerri, C. Viganotti, E. Macchi, S. Baruffi, S. Spaggiari, and B. Taccardi. 1982. The inverse potential problem applied to the human case. *In* Models and Measurements of the Cardiac Electric Field. E. Schubert, editor. Plenum Publishing Corp., New York. 19–33.
8. Wikswo, J. P., Jr., and J. P. Barach. 1982. Possible sources of new information in the magnetocardiogram. *J. Theor. Biol.* 95:721–729.
9. Robb, J. S., and R. C. Robb. 1942. The normal heart. *Am. Heart J.* 23:455–467.
10. Streeter, D. D., Jr. 1979. Gross morphology and fiber geometry of the heart. The cardiovascular system. *In* Handbook of Physiology. Vol. 2. American Physiological Society, Bethesda. 61–112.
11. Wikswo, J. P., Jr. 1983. Theoretical aspects of the ECG-MCG relationship. *In* Biomagnetism, An Interdisciplinary Approach. S. A. Williamson, G. L. Romani, L. Kaufman, and I. Modena, editors. Plenum Publishing Corp., New York. 311–326.
12. MacAulay, C. E., G. Stroink, and B. M. Horacek. 1985. Signal analysis of magnetocardiograms to test their independence. *In* Biomagnetism: Applications and Theory. H. Weinberg, G. Stroink, and K. Katila, editors. Pergamon Press, New York. 115–120.
13. Roth, B. J., and J. P. Wikswo, Jr. 1986. Electrically silent magnetic fields. *Biophys. J.* 50:739–745.
14. Jack, J. J. B., D. Noble, and R. W. Tsien. 1970. Electrical Current Flow in Excitable Cells. Oxford Press, London.
15. Tung, L. 1978. A bidomain model for describing ischemic myocardial d-c potentials. Ph.D. dissertation. Massachusetts Institute of Technology, Cambridge.
16. Geselowitz, D. B., and W. T. Miller III. 1983. A bidomain model for anisotropic cardiac muscle. *Ann. Biomed. Eng.* 11:191–206.
17. Roberts, D. E., L. T. Hersch, and A. M. Scher. 1979. Influences of cardiac fiber orientation on wavefront voltage, conduction velocity and tissue resistivity in the dog. *Circ. Res.* 44:701–712.
18. Clerc, L. 1976. Directional differences of impulse spread in trabecular muscle from mammalian heart. *J. Physiol. (Lond.).* 255:335–346.

19. Plonsey, R., and R. C. Barr. 1984. Current flow patterns in two-dimensional anisotropic bisyncytia with normal and extreme conductivities. *Biophys. J.* 45:557–571.
20. Barr, R. C., and R. Plonsey. 1984. Propagation of excitation in idealized anisotropic two-dimensional tissue. *Biophys. J.* 45:1191–1202.
21. Coburn, B. 1980. Electrical stimulation of the spinal cord: Two-dimensional finite element analysis with particular reference to epidural electrodes. *Med. & Biol. Eng. & Comput.* 18:573–584.
22. Sepulveda, N. G., C. F. Walker, and R. G. Heath. 1983. Finite element analysis of current pathways with implanted electrodes. *J. Biomed. Eng.* 5:41–48.
23. Yamashita, Y., and T. Takahashi. 1984. Use of the finite element method to determine epicardial from body surface potentials under a realistic torso model. *IEEE (Inst. Electr. Electron. Eng.) Trans. Biomed. Eng.* 31:611–621.
24. Pilkington, T. C., M. N. Morrow, and S. C. Stanley. 1985. A comparison of finite element and integral equation formulations for the calculations of electrocardiographic potentials. *IEEE (Inst. Electr. Electron. Eng.) Trans. Biomed. Eng.* 32:166–173.
25. Zienkiewicz, O. C. 1977. The Finite Element Method. McGraw-Hill, New York.
26. Hinton, E., and D. J. R. Owen. 1979. An Introduction to Finite Element Computations. Pineridge Press Ltd., Swansea, UK.
27. Zienkiewicz, O. C., C. Emson, and P. Bettess. 1983. A novel boundary infinite element. *Int. J. Num. Meth. Eng.* 19:393–404.
28. Marques, J. M. M. C., and D. J. R. Owen. 1983. Infinite elements in quasi-static materially nonlinear problems. *Comp. and Struc.* 18:739–751.
29. Plonsey, R., and R. Barr. 1986. A critique of impedance measurements in cardiac tissue. *Ann. Biomed. Eng.* 14:307–329.
30. Lepeschkin, E. 1976. Physiological influences on transfer factors between heart currents and body-surface potentials. *In* The Theoretical Basis of Electrocardiology. C. V. Nelson and D. B. Geselowitz, editors. Oxford University Press, London. 135–161.
31. Roscoe, J. T. 1975. Fundamental Research Statistics for the Behavioral Sciences. Holt, Rinehart and Winston Press, Ames, New York.